



# Effect of nanoclay content on the thermal, mechanical and shape memory properties of epoxy nanocomposites

M. H. Mat Yazik<sup>1</sup> · M. T. H. Sultan<sup>1,2,3</sup> · A. U. M. Shah<sup>2</sup> · M. Jawaid<sup>2</sup> · Norkhairunnisa Mazlan<sup>1,2</sup>

Received: 30 May 2019 / Revised: 25 November 2019 / Accepted: 4 December 2019 /

Published online: 12 December 2019

© Springer-Verlag GmbH Germany, part of Springer Nature 2019

## Abstract

The bright future of shape memory epoxy polymer (SMEP), to be used in critical industries, can be refined by enhancing its properties and overcoming its limitations. Depicting the great performance of nanofillers in polymer composites, their inclusion in SMEP is expected to emphasize the properties of SMEP. In this study, experimental analyses are conducted to study the effects of nanoclay content on the thermal and mechanical properties of SMEP through dynamic mechanical analysis (DMA), thermogravimetric analysis (TGA), transmission electron microscopy (TEM), X-ray diffraction (XRD), flexural testing and shape memory cyclic testing. The epoxy systems, made of EPON 826 and neopentyl glycol diglycidyl ether (NGDE) and incorporated with 1 wt%, 3 wt% and 5 wt% montmorillonite (MMT) nanoclay, are prepared for characterization. It is found that increasing the nanoclay content decreases the glass transition temperature and increases the thermal stability of SMEP, through DMA and TGA, respectively. The highest values of both the storage modulus at glassy region from DMA and the flexural modulus from the flexural testing are observed for the nanocomposites with 3 wt% nanoclay content. The XRD analysis and TEM micrograph support these results. Meanwhile, only a small difference is observed based on TGA data. Addressing the main use of SMEP, the increment of nanoclay content has improved the shape recovery and shape fixity through the shape memory cyclic testing.

**Keywords** Shape memory epoxy · Nanocomposite · Nanoclay · Shape recovery · Flexural · Dynamic mechanical analysis · Thermogravimetric

---

✉ M. T. H. Sultan  
thariq@upm.edu.my

Extended author information available on the last page of the article

## Introduction

Shape memory materials (SMMs) are a group of shape-responsive materials, which can virtually hold a temporary shape forever until the right stimulus is applied to trigger the shape recovery process and return to the original shape. The SMM group can be classified as shape memory alloys (SMAs), shape memory polymers (SMPs), shape memory ceramics (SMCs) and shape memory hybrids (SMHs). The enabler mechanism of shape memory effect (SME) in SMA is the reversible martensitic–austenitic transformation. On the other hand, the SME mechanism in SMP is the dual-domain systems, which are the hard segment and the soft segment. In SMC, the mechanism can either be the reversible phase transformation, similar to SMA, or multiphase systems that resemble those in SMP. Indirectly, SMHs are made out of at least two component materials that have no SME individually, but share the same mechanism as SMP, when coupled.

Although SMA and SMC are the most widely used SMM in industry, there are some apparent disadvantages, such as high mass density, high production cost, low deformation strain, poor resistivity to corrosion and poor processability. Compared with these SMMs, SMP can make up for those disadvantages and are increasingly attracting the interest of researchers from both academia and industry. SMPs can be classified into two groups, according to their chemical structures: thermoset and thermoplastics. These two groups can be distinguished based on their transition temperatures, where thermosets usually have glass transition temperature ( $T_g$ ) as switching temperature, while thermoplastics have either  $T_g$  or crystal melting temperatures  $T_m$  as switching temperature [1].

Over the past few decades, research on shape memory polymer thermoplastics has concentrated on polyurethane (PU) and polystyrene (PS). In contrast, of those materials commonly mentioned in civilian applications, thermoset shape memory epoxies (SMEP) are more suitable to be used in high-intensity industry such as biomedical and aerospace fields, such as spacecraft structures or aircraft wings, due to their high relative performances, in terms of mechanical and thermal properties together with excellent shape memory response. SMEP offers performance advantages similar to aerospace grade epoxies, such as high transition temperatures, industrial durability, excellent dimensional stability, easy processing procedures and, more importantly, high shape fixity and shape recovery ratio.

However, SMEPs have drawbacks such as low strength, low stiffness and low thermal stability, which hinder their usage as functional and structural application materials. At room temperature, polyurethane (SMPU) shows an elastic modulus of about 200 MPa [2], styrene-based SMP shows an elastic modulus of less than 1 GPa [3], while epoxy-based SMP shows an elastic modulus of about 1 GPa [4]. Therefore, some reinforcing procedures are required, to enhance the mechanical and thermal properties of SMEP, while maintaining the shape memory properties of pure SMEP. These include the inclusion of fillers, such as SiC, glass fibres, carbon fibres and graphene. Some of these fillers, such as graphene and carbon nanotubes, are usually expensive, thus limiting their usage on a large scale, while other fillers require a high weight percentage in the composites to significantly

improve the SMP properties. Liu et al. use up to 20 wt% of SiC of 700 nm mean size into SMEP and found out that SiC is a very efficient material to enhance thermal conductivity of SMEP [5]. Some are used to render additional functionality as a result of nanofiller inclusion. Lu et al. renders insulating SMEP to electrical conductive by incorporating hybrid of carbon nanofibre and Ni strand which enable SME activation via resistive heating through Joule effect [6]. The resultant SMEP nanocomposite displays a fast recovery and higher thermal conductivity as a by-product carbon nanofibre inclusion.

Nanoclay is a two-dimensional nanofiller, typically found in a stacked arrangement, from a few layers to as many as one thousand sheets. Montmorillonite (MMT) is the most widely used clay nanofiller. A single sheet of MMT was found to have an in-plane Young's modulus ranging from 178 GPa to 265 GPa [7]. Nanoclay can provide a variety of benefits to the epoxy polymers, such as enhancing their mechanical properties, thermal stability and dimensional stability. The  $T_g$  of epoxies containing nanoclay filler can either increase or decrease, depending on the proportion of nanoclay in the polymers [8]. There has been a report on the effect of nanoclay on the mechanical and thermal properties of epoxy polymer. Wang et al. stated that the addition of silane-modified nanoclay obtained optimum tensile properties at 2 wt%. Moreover, they reported an increase in  $T_g$  for nanoclay content up to 1 wt% and a decrease in  $T_g$  value beyond that [9]. They claimed that the behaviour was due to the complexity of the epoxy/nanoclay interaction system. On the other hand, Ho et al. reported that 5 wt% nanoclay gave the highest ultimate tensile strength in a nanoclay epoxy composite system. They concluded that the addition of nanoclay prohibited the linking up of the epoxy chain network, but it did make the composite stronger and harder [10]. However, Krushnamurthy et al. later showed that the inclusion of 3 wt% nanoclay increased the flexural and tensile strength, while at 5 wt%, these properties decreased due to matrix embrittlement [11]. Lakshmi et al. showed that the incorporation of nanoclay in an epoxy nanocomposite decreased the curing behaviour and  $T_g$  due to the presence of exfoliated nanoclay which restricted polymerization [12].

In this study, the thermal and flexural properties of SMEP were investigated with various weight percentages of nanoclay fillers for application in morphing structures. Shape memory properties of shape memory epoxy polymer composites (SMEPCs) were analysed through shape memory cyclic test, to observe the effect of nanoclay content on the shape fixity and shape recovery over multiple shape memory cycles. Shape fixity and shape recovery provide an indication as to whether the material is suitable or not for cyclic structural application.

## Materials and methods

### Materials

The diglycidyl ether of bisphenol-A aromatic diepoxide monomer (EPON 826), used as hard segment epoxy, and the curing agent, poly(propylene glycol)bis(2-aminopropyl)ether (Jeffamine D-230), were obtained from Hexion and Huntsman,

respectively. The soft segment epoxy used was neopentyl glycol diglycidyl ether (NGDE), an aliphatic diepoxide purchased from TCI America. Chemical structures of the reactants used in SMEP formulation are shown in Fig. 1.

SMEPs can be created due to differences in the chemical structure of both the hard segment and soft segment epoxies. The cross-linking agent in this epoxy composition, Jeffamine D-230, has an amine group,  $\text{-NH}_2$ , that reacts with EPON 826 and NGDE to create cross-links between polymers. The connections occurred at net points which attached to either EPON826 or NGDE chains [13]. Nanomer I.31PS is a surface-modified montmorillonite (MMT) clay with 15–35% octadecylamine and 0.5–5 wt% aminopropyl triethoxysilane obtained from Aldrich Chemistry. MMT was originally hydrophilic due to the presence of hydrated inorganic counterions such as  $\text{Na}^+$  and  $\text{Ca}^{2+}$  and thus only dispersed in polymer with great difficulty. Through surface modification, MMT is made hydrophobic by replacing the counterions with organic cations to become compatible with polymer matrix. The acetone used was dimethyl ketone (2-propanone) obtained from Friendemann Schmidt Chemical (Parkwood, Australia). All materials were used as received without further modification.

### Sample preparation

In order to examine the effect of nanoclay addition to SMEP, both neat SMEP and SMEP nanocomposites (SMEPCs) were fabricated. Details of the formulation of SMEP were obtained from Table 1 in Xie and Rousseau [14]. EPON 826 and NGDE of the same molar ratio were added together and hand-stirred for 5 min to blend the epoxies. Next, the mixture was added to a pre-weighed curing agent, Jeffamine D-230, and hand-stirred for another 5 min. The molar ratio of EPON 826, NGDE and Jeffamine D-230 used was 0.01:0.01:0.01. The mixture was then poured into an aluminium mould and cured in an isothermal stepwise manner in which the

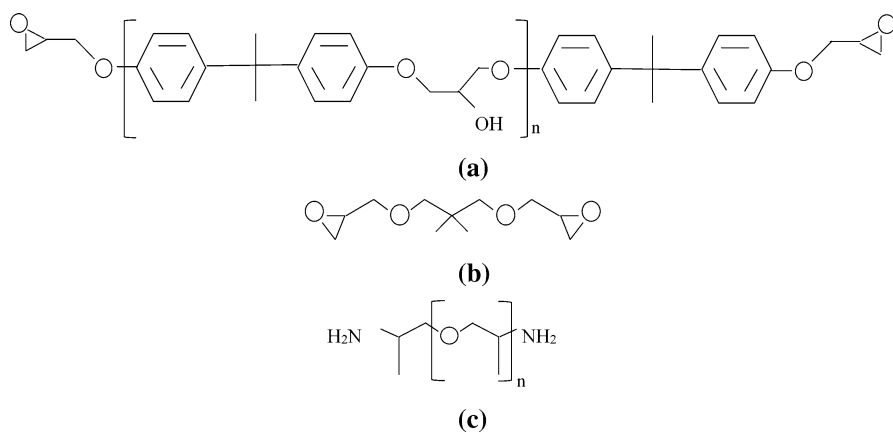


**Fig. 1** Chemical structures of the materials used to obtain the shape memory epoxy polymer [11]: **a** EPON 826, where  $n=0.085$ ; **b** neopentyl glycol diglycidyl ether (NGDE); **c** Jeffamine D-230 where  $n=2.5$ .

temperature was raised 10 °C and maintained for 5 min until it reached curing temperature of 100 °C where it was maintained for 1.5 h and later post-cured for 1 h at 130 °C. During the curing, the sample was observed regularly for any bubble formation.

For fabrication of SMEPC, the following procedure was performed. The nanoclay was first kept in the oven at 120 °C for 24 h to remove moisture. To promote dispersion of the nanoclay, 20% total solution weight of acetone was mixed with the nanoclay in a glass beaker and stirred. To get a homogenous dispersion and prevent segregation in the polymer matrix, the mixture was sonicated for 5 min using a 650 W ultrasonic cell crusher noise isolating chamber at 50% amplitude with 3.0 s start time and 1.0 s pause time. At the same time, EPON826 was heated to 60 °C to reduce the viscosity. The diluted epoxy was added to the nanofiller/acetone mixture and sonicated for another 5 min at 50% amplitude with 3.0 s start time and 1.0 s stop time. Subsequently, the mixture was heated to 65 °C to evaporate the acetone within the mixture. Concurrently, the mixture was vacuumed to remove bubbles with a pressure of 100 kPa for 16–18 h. After the vacuum process, the mixture was cooled to room temperature. NDGE and Jeffamine D-230 were weighed according to their composition percentage. Pre-weighed NGDE and Jeffamine D-230 were added gradually to the mixture and hand-stirred for 5 min. The mixture was then slowly poured into a metal mould and followed the same curing procedure as the neat SMEP described above. Figure 2 shows the schematic diagram of the SMEPC fabrication. In the discussion, SMEPs with nanoclay content of 1 wt%, 3 wt% and 5 wt% are labelled as SMEP–Clay 1%, SMEP–Clay 3% and SMEP–Clay 5%, respectively.

## Experiment and testing

### *Dynamic mechanical analysis*

The dynamic mechanical properties of SMEPC materials were measured using a Q800 dynamic mechanical analyser from TA Instruments (TA Instruments, Inc., New Castle, DE). The analysis was performed in the dual-cantilever mode, from –50 to 150 °C, at a heating rate of 3.0 °C min<sup>-1</sup> and a frequency of 1 Hz. The samples used for this analysis were rectangular, measuring 60 mm × 12 mm × 4 mm for length, width and thickness, respectively. The temperature was controlled with a nitrogen gas cooling system. In this report, only data from 0 °C until 100 °C are presented as it already shows acceptable results.

### *Flexural test*

The mechanical properties of SMEPCs were evaluated using three-point bending flexural testing. The specimens were prepared according to ASTM D790 using a recommended span-to-depth ratio of 16:1. Five specimens were tested for each composite to obtain reliable results using INSTRON 3366 machine (Instron, Norwood, MA). The test was conducted until 20% strain elongation was obtained, or until the specimen started to slip from the clamp. Force and deflection readings were

recorded and analysed using Bluehill software (Instron, Bluehill3, Norwood, MA) for further analysis.

### ***Thermogravimetric analysis***

The information on the effect of nanoclay content on the thermal stability of SMEP and SMEPC was analysed using thermogravimetric analysis (TGA), using TGA Q500 from TA Instrument (TA Instruments, Inc., New Castle, DE) and using samples of mass between 5–10 mg. The test was conducted with a heating rate of  $10\text{ }^{\circ}\text{C min}^{-1}$ , from room temperature up to  $600\text{ }^{\circ}\text{C}$ , in a nitrogen atmosphere.

### ***X-ray diffraction***

The dispersion of nanofiller layers was analysed by the X-ray diffraction (XRD) method at a voltage of 40 kV and a current of 40 mA with radiation ( $\lambda = 0.154\text{ nm}$ ). The scanning was conducted with a scanning step of  $0.033^{\circ}$  in the  $2\theta$ , ranging from  $4^{\circ}$  to  $90^{\circ}$ . The results were extracted and analysed using PANanalytical's Xpert Highscore software (PANanalytical, Almelo, NED).

### ***Transmission electron microscopy***

Ultrathin film with a thickness about 100 nm was prepared for field emission transmission electron microscopy (FETEM) by cutting from trimmed surface using a diamond knife with Leica EM UC7 Ultramicrotome (Leica Mikrosysteme GmbH, Vienna, Austria) at room temperature under dry condition. The section was then collected on a carbon-coated Cu grid with 300 mesh. JEM-2100F multipurpose FETEM (JEOL Ltd, Japan) operating at 200 kV was used for morphological analysis of the sample.

### ***Shape Memory Effect Analysis***

SME behaviour of SMEP and SMEPC samples was evaluated in a force-controlling mode on the Q800 DMA machine following the method used elsewhere [15]. The procedure consisted of a four-step cycle. Initially, the sample was heated up to above its  $T_g$  value,  $T_1$  and maintained for 10 min. The first step of the cycle, a static stress,  $\sigma_{\text{prog}}$  was applied to the samples while maintaining its temperature. In the second step, sample was cooled down to below its  $T_g$  value,  $T_2$  at a rate of  $5\text{ }^{\circ}\text{C min}^{-1}$  under the load. These two steps completed the programming process of the temporary shape. For the third step, the stress was unloaded at a uniform rate under the temperature of  $T_2$ . In the final step, the sample was heated up again to  $T_1$  at a uniform rate of  $5\text{ }^{\circ}\text{C min}^{-1}$ . The latest two steps completed the recovery of original shape and marked the completion of the shape memory cycle. In this research,  $T_1 = 70\text{ }^{\circ}\text{C}$ ,  $T_2 = -10\text{ }^{\circ}\text{C}$  and  $\sigma_{\text{prog}} = 1.5\text{ N}$  were used. The completed cycle was repeated four times, and the strain response of the SMEP and SMEPC was recorded. Shape fixity ( $R_f$ ) in terms of strain and strain recovery ( $R_r$ ) were calculated as follows [14, 15]:

$$R_f = \varepsilon_{\text{load}} / \varepsilon_{\text{fix}} \times 100\%$$

$$R_r = \left( 1 - (\varepsilon_{\text{rec}} - \varepsilon_{(\text{rec}-1)}) / (\varepsilon_{\text{max}} - \varepsilon_{(\text{rec}-1)}) \right) 100\%$$

where  $\varepsilon_{\text{load}}$  is the immediate strain upon loading (first process),  $\varepsilon_{\text{fix}}$  is the strain after cooling and load removal (third process),  $\varepsilon_{\text{rec}}$  is the strain after recovery (final process),  $\varepsilon_{(\text{rec}-1)}$  is the recovered strain in the previous cycle and  $\varepsilon_{\text{max}}$  is the maximum achieved strain in the cycle.

## Results and discussion

### *Dynamic mechanical analysis results*

The dynamic mechanical analysis was performed to investigate the thermomechanical properties and the glass transition temperature of SMEP and SMEPC. The dynamic stress and the corresponding strain provided a complex modulus with a real part (storage modulus) and an imaginary part (loss modulus), where the real part represented the elastic portion of the polymer and its ability to store elastic energy, and the imaginary part represented the viscous portion of the polymer. Judgement as to whether the polymer exhibited shape memory effects or not was obtained from its DMA result curve. Ideally, a shape memory polymer will show a drop of 2–3 orders of magnitude of elastic modulus upon heating, before reaching a plateau of that modulus [16]. Figure 3 compares the storage modulus of the SMEPC with different nanoclay contents.

The transition feature shows an obvious drop of more than two orders of magnitude in the storage modulus of each SMEPC from a glassy state to a rubbery state. As can be seen, SMEP–Clay 3% has the highest glass modulus followed by SMEP–Clay 1% and SMEP–Clay 5% accordingly.

Loss modulus plotted in Fig. 4 represents the heat dissipated in the viscous portion of SMEP.

It was assumed that the peak on the graph was due to cold crystallization where the glass region transitioned to the rubbery region [17]. The loss modulus of SMEP–Clay 1% had the lowest peak of all the nanocomposites, whereas SMEP–Clay 3% and SMEP–Clay 5% had almost similar peak values, with SMEP–Clay 5% slightly higher, but occurring at a different temperature. This may be due to restriction of the molecular chain in the amorphous region resulting from nanoclay inclusion in the sample.

The transition temperature of each sample, represented by the peak of tan delta, is shown in Fig. 5, and the extracted values are tabulated in Table 1

The  $T_g$  value for SMEP was reported to be 55.8 °C. As shown in Fig. 5, the tan delta peak shifted to lower temperatures with increasing nanoclay content. The decrease in  $T_g$  of SMEPC may be due to a non-stoichiometric equilibrium between the epoxies (EPON 826 and NGDE) and the curing agent since there was a presence of alkyl ammonium ions on the nanoclay. These ammonium ions act as a plasticizer which results in lower cross-link density of the cured epoxy. The long chain of

**Table 1** Transition temperature of SMEPC

	Peak	$T_g$ (°C)
SMEP	0.948	55.8
SMEP–Clay 1%	1.039	52.2
SMEP–Clay 3%	1.127	49.1
SMEP–Clay 5%	1.137	44.1

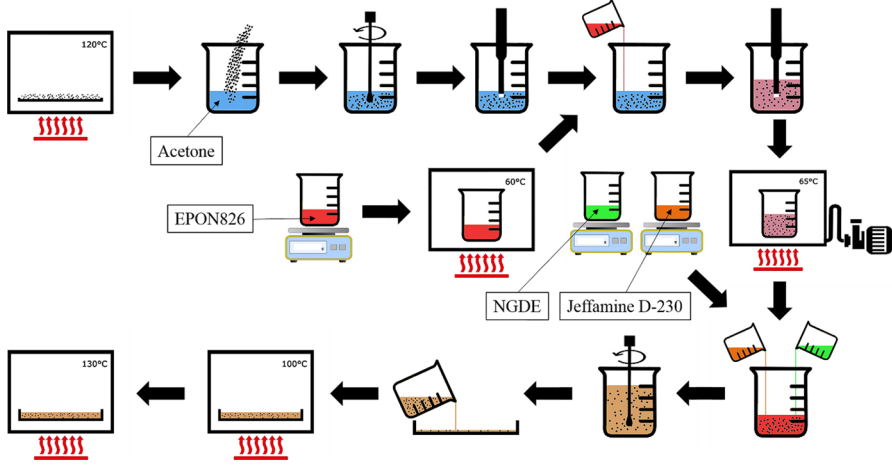


**Fig. 2** Schematic diagram of shape memory epoxy nanocomposite fabrication process

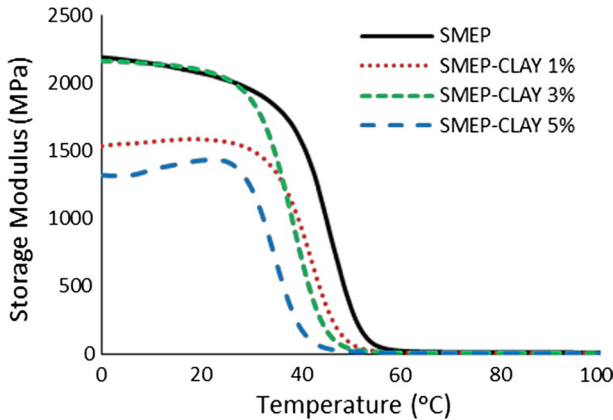


**Fig. 3** Storage modulus of SMEPC with respect to temperature

amine was released from the nanoclay through dissociation during the curing process [18]. This low molecular weight amine could act as a plasticizer and decrease the  $T_g$ . Therefore,  $T_g$  decreased at higher nanoclay loading [19]. The decrease in



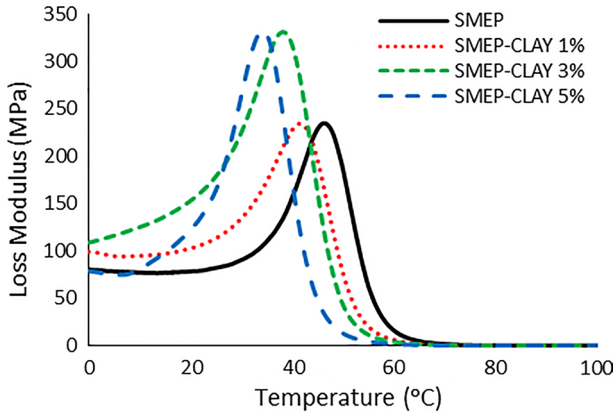


Fig. 4 Loss modulus of SMEPC with respect to temperature

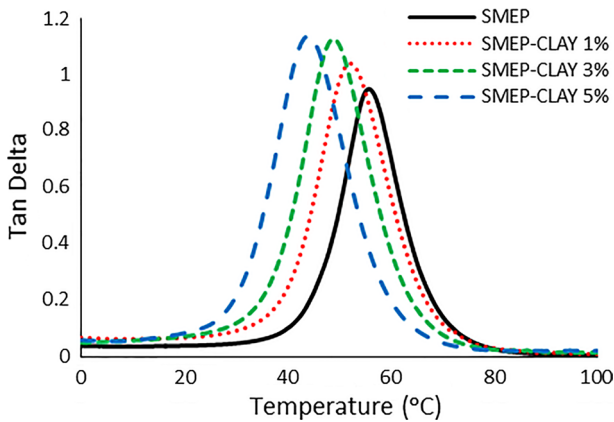
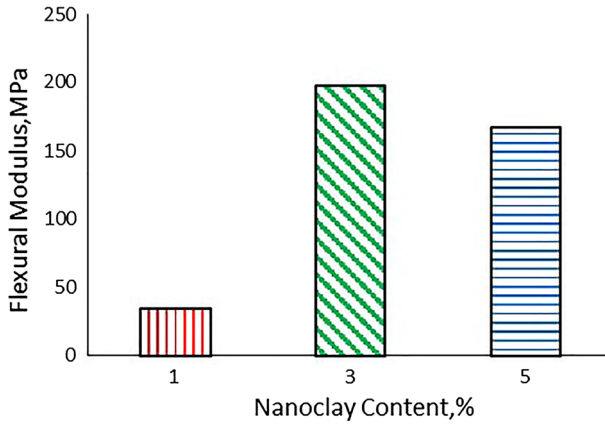


Fig. 5 Tan delta of SMEPC with respect to temperature

$T_g$  may be attributed to the presence of octadecylamine in the modified clay. The aliphatic amine has a long linear chain that is very flexible and has low thermal stability [20]. This was also observed in the previous study by Huong et al. [21]. Addition of nanoclay into the polymer matrix had a dual possible effect on the thermal stability. On the one hand, it provided a barrier effect for heat and mass transfer, which, in turn, improved thermal stability. On the other hand, addition of nanoclay encouraged the degradation of the polymer matrix which resulted in the decrement of thermal stability [22]

**Flexural Test Result**

Figures 6 and 7 show the effect of increasing nanoclay content on the flexural properties of SMEP composite.



**Fig. 6** Flexural modulus as a function of nanoclay loading in SMEPC

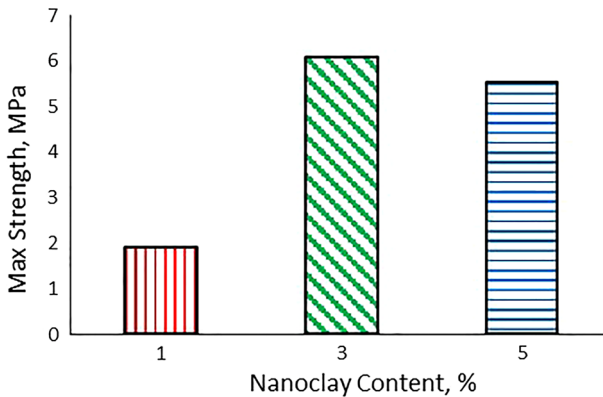


**Fig. 7** Maximum strength as a function of nanoclay content in SMEPC

Increasing the content of nanoclay in the polymer matrix increased the flexural modulus of SMEPC almost fourfold. It is believed that the improvement was due to the reinforcing effect of nanoclay on the epoxy matrix. The mechanical properties of nanocomposites strongly depend on the dispersion of nanoclay in the matrix. A higher degree of nanoclay exfoliation produces a higher aspect ratio platelet. Platelet edges of the clay layer act as a fragile point and are prone to high stress concentrations [23]. Increasing the aspect ratio of the filler will produce lower stress concentration points, which results in higher stress transfer between the matrix and nanofiller layers [24, 25]. This increases the rigidity of the matrix and withstands bending load effectively. Note that the reinforcing effect of incorporating the filler achieved its maximum at 3% nanoclay content. Above this filler loading, the flexural modulus slightly decreased, due to the embrittlement of the SMEPC matrix, resulting from stress concentration at the agglomeration area. These test results were in good

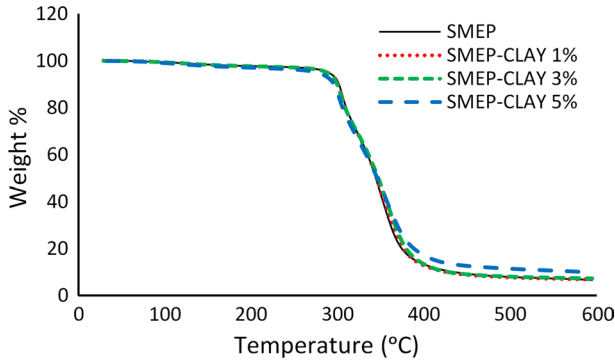


**Fig. 8** Thermogravimetric analysis (TGA) curve of SMEP and SMEPC

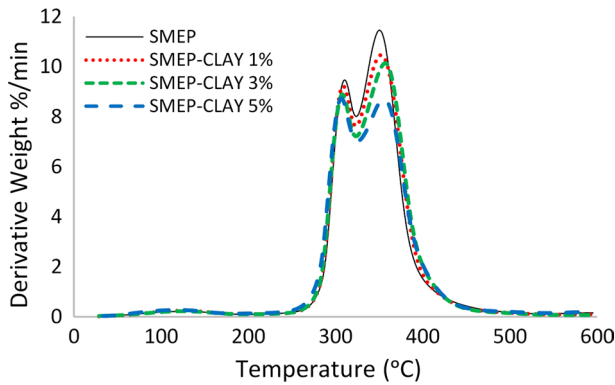


**Fig. 9** Differential thermogravimetric (DTG) curve of SMEP and SMEPC

agreement with previous nanoclay studies ([11] and [26]), although they were using a different epoxy system.

**Thermogravimetric analysis results**

Figures 8 and 9 show the decomposition curve of SMEP and SMEPC from room temperature up to a temperature of 600 °C.

In Fig. 8, it was seen that the decomposition trend of all SMEPC is almost the same compared to neat SMEP. As shown in Fig. 9, the process can be divided into three stages, with the initial stage of decomposition occurring around 100 °C due to the elimination of water molecules through dehydration and vaporization of moisture [27]. The major weight loss occurred around 310 °C and 350 °C, due to the decomposition of SMEP cross-linking chemical bonds in the polymer matrix. As the content of aromatic epoxide was higher than the aliphatic epoxide, the peak degradation rate was more noticeable as shown in Fig. 9. The decomposition of nanoclay particles obtained from the literature stated that the maximum degradation rate

occurs at 367.5 °C [28]. This value was close to the maximum degradation temperature of the aliphatic epoxide. This caused a reduction in the maximum degradation rate, in which the influence becomes more significant as the nanoclay content increased. To further analyse the TGA result, the temperature at various weight percentages was obtained, as shown in Table 2.

$T_{10\%}$ ,  $T_{50\%}$  and  $T_{90\%}$  represent the temperature that decomposed 10%, 50% and 90% of the initial mass of the sample. It can be seen that all SMEPCs have lower decomposition at 10% with SMEP–Clay 5% requiring the lowest temperature to decompose 10% of its mass. The  $T_{50\%}$  point for all SMEPCs showed similar temperatures to SMEP, whereas at  $T_{90\%}$ , a large deviation in temperature was observed among the nanocomposites. SMEP–Clay 5% required the highest temperature to lose 90% of its initial mass due to a lower maximum decomposition rate at major weight reduction stages as previously explained. The small difference in decomposition temperature for SMEPC at  $T_{10\%}$  and  $T_{50\%}$  shows that the thermal properties are not affected by addition of nanoclay at those temperatures. This was also concluded by Moraweic in a study to observe the effect of nanoclay content on nanocomposite [29]. The effect of nanoclay content is only observed at high decomposition point. It is also worth noting that the SMEP–Clay 5% residue left at the end of TGA was the highest among all the samples tested. This is due to the enhanced thermal stability provided by the nanoclay and due to the fact that higher contents of nanoclay were incorporated in the SMEPC. At low nanoclay content, exfoliation dominates the matrix. However, the number of exfoliated particles was not high enough to enhance thermal stability through char formation. Increasing the nanofiller content has increased the amount of exfoliated particles and promotes easier char formation, thus increasing the thermal stability of the SMEPC.

### X-ray diffraction results

The dispersion of nanoclay was determined by XRD tests. The intensity obtained at each  $2\theta$  position is plotted in Fig. 10

The plot shown in Fig. 10 was offset to clearly show the graph of each sample. Nanoclay powder shows obvious peak intensity at  $2\theta=4.2^\circ$  which corresponds to  $d_{001}=21$  Å, while secondary and tertiary peaks at  $2\theta$  approximately  $19.8^\circ$  and  $22^\circ$ , respectively. This peak trend is the characteristic of nanoclay powder. The XRD result of neat SMEP was also shown for comparison. As can be seen, the intensity plot of SMEPC shows all the peak patterns that correspond to the neat SMEP. The broad peak at  $2\theta$  about  $18.2^\circ$  was due to the neat SMEP. It is observed that

**Table 2** TGA weight loss temperature of SMEP and SMEPC

	$T_{10\%}$ (°C)	$T_{50\%}$ (°C)	$T_{90\%}$ (°C)	Residue (%)
SMEP	301	344	435	6.67
SMEP–Clay 1%	299	346	490	8.37
SMEP–Clay 3%	299	346	533	9.41
SMEP–Clay 5%	296	345	592°C	9.97

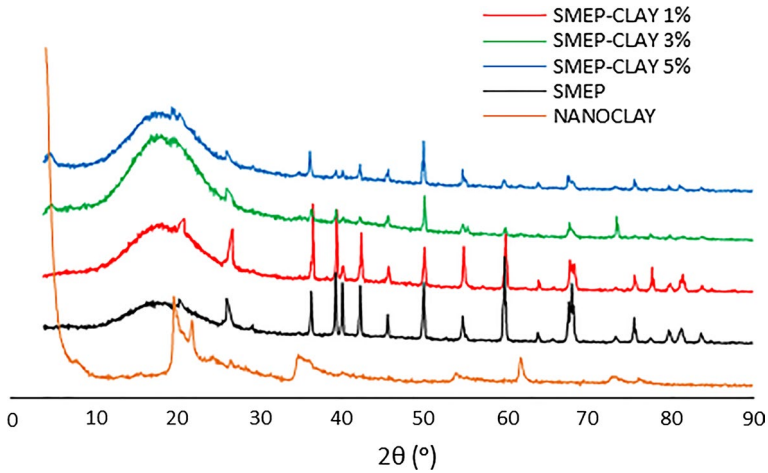


**Fig. 10** Diffraction intensity of nanoclay, SMEP and SMEPC

this peak is sharper and narrower for SMEP–Clay 3%, indicating better crystallinity. This explains the storage modulus observed in the DMA data below the transition temperature. A weak peak at  $2\theta=4.8^\circ$  that corresponds to  $d_{001}=18.4 \text{ \AA}$  is observed in SMEP–Clay 3% and SMEP–Clay 5%, which shows a characteristic of nanoclay peak. Absent in peak related to nanoclay particle observed in the SMEP–Clay 1% suggests either an exfoliated or intercalated structure with interlayer distance exceeding  $22 \text{ \AA}$  [30]. This is the limit of XRD detection. This expresses that the nanoclay layers in the SMEP matrix were not stacked regularly and successfully incorporated inside the SMEP matrix. A successful exfoliation of nanoclay layers is important in nanocomposites to ensure full exploitation of the nanoclay properties. The presence of aggregation in which the nanoclay layers are structured and stacked inside the polymer matrix will act as a stress concentration and lead to catastrophic failure upon external stress. However, XRD data may not fully reveal the state of dispersion of nanoparticle because some clay particles may not exhibit obvious basal reflection and it is vague to determine the peak intensity pattern and shape. Hence, XRD data are usually complimented with TEM observation which provides direct visualization of the clay particle structures.

### **Transmission electron microscopy analysis**

The dispersion state of SMEPC can be observed directly through TEM micrograph as shown in Fig. 11. The dark lines shown in the image are a dispersed nanoclay layer with a thickness of a few nanometres and a lateral size of around 200–300 nm within the epoxy matrix. The micrographs show difference state of dispersion on SMEP–Clay 3% and SMEP–Clay 5%. The epoxy (bright line) is seen penetrated between the clay layers (dark layer). In micrograph of SMEP–Clay 3%, the nanoclay is exfoliated where nanoclay layers exist in few layers. Micrograph of SMEP–Clay 5% shows a large stack of nanoclay in intercalated state. The TEM clearly shows

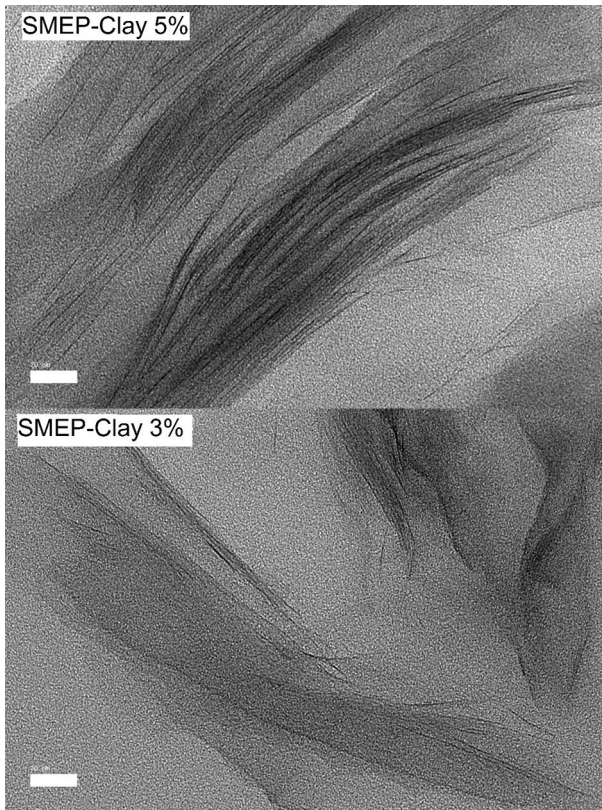


**Fig. 11** TEM micrograph of SMEPC containing 3% and 5% nanoclay. Scale bar shows 20 nm

poor nanoclay exfoliation in the SMEPC with high nanoclay content due to particle agglomeration and increased viscosity of the resin–nanoparticle mixture. In SMEP–Clay 3%, there are parallel oriented platelets possibly formed from the collapse of exfoliated layers in the matrix. These layers appear at some areas in the epoxy matrix. The spacing between layers of nanoclay is smaller in SMEP–Clay 5% than that in SMEP–Clay 3%. However, these differences are not produced in the XRD peak probably due to different orientation or misalignment of platelets exist in the matrix as seen in the SMEP–Clay 3% micrograph. This was observed in the previous study [31].

### ***Shape memory effect test results***

Shape memory performances of SMEPC were evaluated using DMA to observe the effect of nanoclay content on SMEP. Two values were obtained from this test, shape fixity and shape recovery, which basically indicate the sample's performance in the programming process and the recovery process, respectively. Figure 12 shows the shape fixity of each sample in six consecutive cycles.

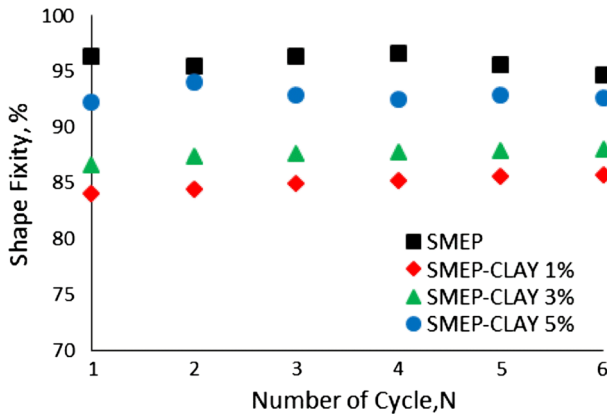


Fig. 12 Percentage shape fixity of SMEP and SMEPC composite for six consecutive cycles

The results indicate that the inclusion of nanoclay in SMEP reduced the shape fixity. It was shown that SMEPC was unable to maintain its shape after the deformation force was removed at the end of its programming process. Increasing the nanoclay content increased the shape fixity percentage, where SMEP–Clay 5% performed only slightly lower than pure SMEP. This is probably due to the interaction between nanoparticle and the matrix cross-link above the transition temperature. Higher nanoclay content would hinder cross-link movement during the programming process which increases the shape fixity. If an accurate shape is required for specific functionality, a sample with shape fixity and shape recovery close to 100% is considered the better choice for application in various industries [32, 33]. Figure 13 shows the shape recovery of each sample in six consecutive cycles.

From Fig. 13, it was seen that the shape recovery percentage of SMEPC reached a stable value after only two cycles. Its value started at a lower percentage and significantly increased to almost 100% in the first cycle. SMEP, however, only managed

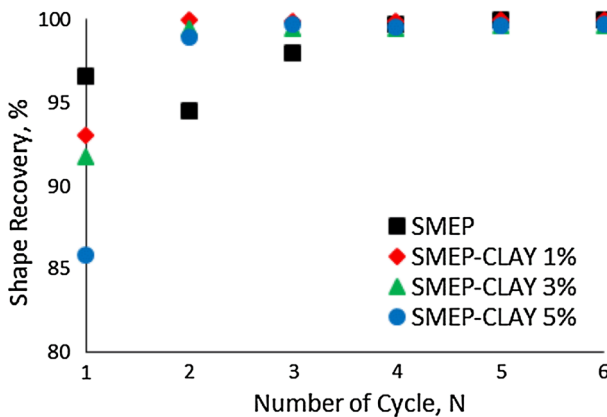


Fig. 13 Percentage shape recovery of SMEP and SMEPC composite for six consecutive cycles

to obtain a stable shape recovery after three cycles. This behaviour is normal of a shape memory material property as it goes a ‘learning process’ where some of the cross-link points are broken, which prevents free movement of the cross-link chain and leads to reduced recovery. The recovery strain then stabilize as the structure function as soft segment, thus increasing the recovery [34]. The result can be used to interpret the functional fatigue and material stability of SMEPC. The cyclic shape memory test provides a qualitative measure of fatigue behaviour of SMEP and SMEPC composites in terms of thermally induced shape memory effects as previously studied in [35] and [36]. Extensive shape memory studies are required to confirm the stability of SMEPC, but these test results can serve as an initial performance indicator.

As far as shape memory properties are concerned, the nanocomposites fabricated are proven to have good recovery properties for cyclic structural applications [37]. This performance provides a good indication as a candidate in applications such as morphing skin or deployable space structure. In this research, SMEPs were not strengthened by any synthetic or natural fibre. However, it shows great potential as cyclic structural application. Further research will look into reinforcing SMEPC composite with synthetic fibre such as carbon fibre and glass fibre or natural fibre such as bamboo and kenaf [38] for cyclic structural application.

## Conclusions

Montmorillonite nanoclay particles with different weight contents were added to shape memory epoxy polymer (SMEP). The nanocomposites produced were characterized via dynamic mechanical analysis (DMA), thermogravimetric analysis (TGA), transmission electron microscopy (TEM), X-ray diffraction (XRD), and flexural and shape memory effect tests. XRD showed that the nanoclay particles have different dispersion states between the nanocomposites. SMEPC with 5% nanoclay content shows a small characteristic peak that resembled the pristine nanoclay intensity pattern. This is supported by TEM micrograph which shows the presence of stacked intercalated nanoclay layer. The flexural test showed that SMEP–Clay 3% had the highest flexural modulus. This result was in parallel with the DMA test as the storage modulus of SMEPC at the glassy state showed the same trend. On the other hand, the thermal properties of SMEPC showed different trends to the mechanical properties. TGA results show that increasing the nanoclay content in the SMEP system produced SMEPCs with increasing thermal properties due to the enhancement from nanoclay. SMEPC with 5% nanoclay content performed the best among the SMEPC, with the highest T<sub>90%</sub> temperature and lowest decomposition rate at major weight loss process. However, DMA showed a decrease in  $T_g$  value due to an increasing number of alkyl ammonium ions from the nanoclay particles. Shape memory testing indicated lower shape recovery and shape fixity properties than neat SMEP. The shape memory performance increased as nanoclay content increased due to the inclusion of the nanoclay. However, further investigation is needed regarding the shape memory cycle in order to quantitatively determine the durability of the SMEPC for smart material applications such as morphing structures or biomedical



devices. Enhancement can be made to the SMEPC via hybridization with other nanofillers such as carbon nanotube or woven fibre such as synthetic fibre or natural fibre.

**Acknowledgements** This work is supported by UPM under GP-IPS Grant 9647200. The authors would like to express their gratitude and sincere appreciation to the Department of Aerospace Engineering, Faculty of Engineering, Universiti Putra Malaysia and Laboratory of Biocomposite Technology, Institute of Tropical Forestry and Forest Products (INTROP), Universiti Putra Malaysia (HiCOE), for the close collaboration in this research.

## References

1. Liu Y, Zhao J, Zhao L et al (2016) High Performance Shape Memory Epoxy/Carbon Nanotube Nanocomposites. *ACS Appl Mater Interfaces*. <https://doi.org/10.1021/acsami.5b08766>
2. Gunes IS, Cao F, Jana SC (2008) Evaluation of nanoparticulate fillers for development of shape memory polyurethane nanocomposites. *Polymer (Guildf)* 49:2223–2234. <https://doi.org/10.1016/j.polymer.2008.03.021>
3. Tandon GP, Goecke K, Cable K, Baur J (2009) Durability assessment of styrene- and epoxy-based shape-memory polymer resins. *J Intell Mater Syst Struct* 20:2127–2143. <https://doi.org/10.1177/1045389X09348255>
4. Gall K, Dunn ML, Liu Y et al (2002) Shape memory polymer nanocomposites. *Acta Mater* 50:5115–5126
5. Liu Y, Gall K, Dunn ML, McCluskey P (2004) Thermomechanics of shape memory polymer nanocomposites. *Mech Mater* 36:929–940. <https://doi.org/10.1016/j.mechmat.2003.08.012>
6. Lu H, Gou J, Leng J, Du S (2011) Synergistic effect of carbon nanofiber and sub-micro filamentary nickel nanostrand on the shape memory polymer nanocomposite. *Smart Mater Struct*. <https://doi.org/10.1088/0964-1726/20/3/035017>
7. Chen B, Evans JRG (2006) Elastic moduli of clay platelets. *Scr Mater* 54:1581–1585. <https://doi.org/10.1016/j.scriptamat.2006.01.018>
8. Alexandre M, Dubois P (2000) Polymer-layered silicate nanocomposites: preparation, properties and uses of a new class of materials. *Mater Sci Eng R Rep* 28:1–63. [https://doi.org/10.1016/S0927-796X\(00\)00012-7](https://doi.org/10.1016/S0927-796X(00)00012-7)
9. Wang L, Wang K, Chen L et al (2006) Preparation, morphology and thermal/mechanical properties of epoxy/nanoclay composite. *Compos Part A Appl Sci Manuf* 37:1890–1896. <https://doi.org/10.1016/j.compositesa.2005.12.020>
10. Ho MW, Lam CK, Lau KT et al (2006) Mechanical properties of epoxy-based composites using nanoclays. *Compos Struct* 75:415–421. <https://doi.org/10.1016/j.compstruct.2006.04.051>
11. Krushnamurty K, Srikanth I, Rangababu B et al (2015) Effect of nanoclay on the toughness of epoxy and mechanical, impact properties of E-glass-epoxy composites. *Adv Mater Lett* 6:684–689. <https://doi.org/10.5185/amlett.2015.5817>
12. Lakshmi MS, Narmadha B, Reddy BSR (2008) Enhanced thermal stability and structural characteristics of different MMT-clay/epoxy-nanocomposite materials. *Polym Degrad Stab* 93:201–213. <https://doi.org/10.1016/j.polymdegradstab.2007.10.005>
13. Lendlein A, Kelch S (2002) Shape-memory effect from permanent shape. *Angew Chemie* 41:2034–2057
14. Xie T, Rousseau IA (2009) Facile tailoring of thermal transition temperatures of epoxy shape memory polymers. *Polymer (Guildf)* 50:1852–1856. <https://doi.org/10.1016/j.polymer.2009.02.035>
15. Chen T. Characterization of Shape Memory Polymers by DMA. *Surgery* 13:14
16. Liu C, Qin H, Mather PT (2007) Review of progress in shape-memory polymers. *J Mater Chem* 17:1543. <https://doi.org/10.1039/b615954k>
17. Shah AU, Sultan MTH, Jawaid M (2019) Sandwich-structured bamboo powder/glass fibre-reinforced epoxy hybrid composites – Mechanical performance in static and dynamic evaluations. *J Sandw Struct Mater*. <https://doi.org/10.1177/1099636218822740>

18. Miyagawa H, Rich MJ, Drzal LT (2005) Thermophysical properties of anhydride-cured epoxy/nano-clay composites. *Polym Compos* 26:42–51. <https://doi.org/10.1002/pc.20071>
19. Karippal JJ, Murthy HN, Rai KS et al (2011) Study of mechanical properties of epoxy/glass/nano-clay hybrid composites. *J Compos Mater* 45:1893–1899. <https://doi.org/10.1177/0021998310389087>
20. Fröhlich J, Golombowski D, Thomann R, Mülhaupt R (2004) Synthesis and characterisation of anhydride-cured epoxy nanocomposites containing layered silicates modified with phenolic alkylimidazolineamide cations. *Macromol Mater Eng* 289:13–19. <https://doi.org/10.1002/mame.20030204>
21. Huang NTP, Crosky A, Qi B et al (2005) Effect of Nanoclay Content on Mechanical Behaviour of TGDDM Epoxy Nanocomposites. *NSTI Nanotechnol* 2:79–82
22. Shahabadi SIS, Garmabi H (2012) Qualitative assessment of nanoclay dispersion using thermogravimetric analysis: a response surface study. *J Thermoplast Compos Mater*. <https://doi.org/10.1177/0892705712452742>
23. Selvakumar V, Manoharan N (2014) Thermal properties of polypropylene / montmorillonite nanocomposites. *Indian J Sci Technol* 7:136–139
24. Nor AFM, Sultan MTH, Jawaid M et al (2019) Analysing impact properties of CNT filled bamboo/glass hybrid nanocomposites through drop-weight impact testing, UWPI and compression-after-impact behaviour. *Compos Part B Eng* 168:166–174. <https://doi.org/10.1016/j.compositesb.2018.12.061>
25. Ismail KI, Sultan MTH, Shah AUM et al (2019) Low velocity impact and compression after impact properties of hybrid bio-composites modified with multi-walled carbon nanotubes. *Compos Part B Eng* 163:455–463. <https://doi.org/10.1016/j.compositesb.2019.01.026>
26. Mazlan N, Azhar AB, Shyang CW (2008) Effects of organo-montmorillonite on the mechanical and morphological properties of epoxy/glass fiber composites. *Polym Int* 57:171–180
27. Zakikhani P, Zahari R, Sultan MTH, Majid DL (2016) Thermal degradation of four bamboo species. *BioResources* 11:414–425. <https://doi.org/10.15376/biores.11.1.414-425>
28. Chow WS, Teoh EL (2015) Flexible and flame resistant poly(lactic acid)/organomontmorillonite nanocomposites. *J Appl Polym Sci* 132:1–11. <https://doi.org/10.1002/app.41253>
29. Morawiec J, Pawlak A, Slouf M et al (2005) Preparation and properties of compatibilized LDPE/ organo-modified montmorillonite nanocomposites. *Eur Polym J* 41:1115–1122
30. Bashar MT, Mertiny P, Sundararaj U (2014) Effect of nanocomposite structures on fracture behavior of epoxy-clay nanocomposites prepared by different dispersion methods. *J Nanomater*. <https://doi.org/10.1155/2014/312813>
31. Yasmin A, Abot JL, Daniel IM (2003) Processing of clay/epoxy nanocomposites by shear mixing. *Scr Mater* 49:81–86. [https://doi.org/10.1016/S1359-6462\(03\)00173-8](https://doi.org/10.1016/S1359-6462(03)00173-8)
32. McClung AJW, Tandon GP, Air JWB (2011) Fatigue cycling of shape memory polymer resin. In: Proulx T (eds) *Mechanics of time-dependent materials and processes in conventional and multifunctional materials*, vol 3. Springer, New York, pp 119–127. <https://doi.org/10.1007/978-1-4614-0213-8>
33. Kikuta MT (2003) *Mechanical Properties of Candidate Materials for Morphing Wings*. Dissertation, Virginia Tech
34. Xu B, Fu YQ, Ahmad M et al (2010) Thermo-mechanical properties of polystyrene-based shape memory nanocomposites. *J Mater Chem* 20:3442–3448. <https://doi.org/10.1039/b923238a>
35. Mogharebi S, Kazakeviciute-Makovska R, Steeb H et al (2013) On the cyclic material stability of shape memory polymer. *Materwiss Werksttech* 44:521–526. <https://doi.org/10.1002/mawe.20130023>
36. McClung AJW, Tandon GP, Baur JW (2013) Deformation rate-, hold time-, and cycle-dependent shape-memory performance of Veriflex-E resin. *Mech Time-Dependent Mater* 17:39–52. <https://doi.org/10.1007/s11043-011-9157-6>
37. Salman SD, Sharba MJ, Leman Z et al (2016) Tension-compression fatigue behavior of plain woven. *BioResources* 11:3575–3586
38. Salman SD, Leman Z, Sultan MTH et al (2015) Kenaf/synthetic and kevlar®/cellulosic fiber-reinforced hybrid composites: a review. *BioResources* 10:8580–8603

**Publisher's Note** Springer Nature remains neutral with regard to jurisdictional claims in published maps and institutional affiliations.

## Affiliations

**M. H. Mat Yazik<sup>1</sup> · M. T. H. Sultan<sup>1,2,3</sup> · A. U. M. Shah<sup>2</sup> · M. Jawaid<sup>2</sup> · Norkhairunnisa Mazlan<sup>1,2</sup>**

M. H. Mat Yazik  
hasfanizamyazik@gmail.com

A. U. M. Shah  
ainumaira91@gmail.com

M. Jawaid  
jawaid@upm.edu.my

Norkhairunnisa Mazlan  
norkhairunnisa@upm.edu.my

- <sup>1</sup> Department of Aerospace Engineering, Faculty of Engineering, Universiti Putra Malaysia, 43400 Serdang, Selangor, Malaysia
- <sup>2</sup> Laboratory of Biocomposite Technology, Institute of Tropical Forestry and Forest Products (INTROP), Universiti Putra Malaysia, 43400 Serdang, Selangor, Malaysia
- <sup>3</sup> Aerospace Malaysia Innovation Centre (944751-A), Prime Minister's Department, MIGHT Partnership Hub, Jalan Impact, 63000 Cyberjaya, Selangor, Malaysia